A Scheme on Pedestrian Detection using Multi-Sensor Data Fusion for Smart Roads

Hui Wang, Changle Li*, Yao Zhang, Zhao Liu, Yilong Hui and Guoqiang Mao
State Key Laboratory of Integrated Services Networks, Xidian University, Xi'an, China
*clli@mail.xidian.edu.cn

***Abstract*—Transforming our roads into smart roads is an indispensable step towards future self-driving systems, and therefore has drawn increasing attention from both academia and industry. To this end, this paper develops a novel cost-effective IoT-based target detection system utilizing the multi-sensor data fusion technology with a particular focus on pedestrian detection, as an important component of smart road system. Particularly, the developed intelligent pedestrian detection module (iPDM) consists of three major sensors, *i.e.*, Doppler microwave radar sensor, passive infrared (PIR), and geomagnetic sensor. A multi-sensor data fusion algorithm is developed to fuse the sensor data and achieves reliable target detection. After that, iPDM sends the relevant warning signal wirelessly to nearby base station and vehicles. Experiments are conducted on real traffic environment to evaluate the performance of iPDM. The results validate the high reliability of iPDM with an average 91.7% detection accuracy. Moreover, to our best knowledge, iPDM is the first IoT-based implementation for pedestrian detection of smart roads. It is necessary to highlight that iPDM is a low-cost, low-power, wide-coverage pedestrian detection system where the cost of a single iPDM is only US $30, which makes it suitable to large-scale deployment.**

I. Introduction

It is reported that the pedestrian fatalities increased over 30% annually from 2009 to 2016 with approximately 6,000 pedestrians killed and injured in the USA in 2016 [1], [2]. Many experts claim advances in vehicle automation will significantly address this public health crisis, citing the statistic that 94% of traffic fatalities are due to human error, and arguing that fully automated vehicles (AVs) will eliminate these error-caused fatalities [3]. However, due to the limited perception range and detection capability of AVs, the reliability and safety of AVs cannot be guaranteed in some complex traffic scenarios, for instance, the fatality of a pedestrian in March 2018 Uber crash, and the fatality of a Tesla driver who ignored several safety warning from his vehicle [4]. In addition, most of the existing roadside pedestrian detection devices rely on cameras, radar and human intervention, resulting in high cost and high detection error rate.

This work focuses on developing a cost-effective IoT-based pedestrian detection system, in order to support autonomous driving. Accurate and reliable pedestrian detection in intricate road environment and poor weather conditions is well known to be a difficult task. The reason is that pedestrians have variable physical characteristic and appear in a variety of environments with different background features, obstacle and weather condition. The detection system relying on vehicle on-board sensor only fails to identify pedestrians reliably in unfavorable conditions, especially for moving pedestrians who are too far or too close to the vehicle, partially occluded by nearby objects, or beyond line-of-sight detection range of vehicles [5]. Machine learning is a widely used method in pedestrian detection, which however needs large-volume of video data as input to extract meaningful feature vectors with a relatively long training and testing time [1], [6]. Furthermore, researchers also investigated pedestrian detection using a portable Doppler radar system or passive infrared (PIR) sensors. These low-cost sensors has been widely applied for human detection, access control and alarm monitoring in low-noise environments [7], [8]. However the performance of Doppler radar-based system is known to suffer in rain and other poor weather and PIR sensors fail to detect humans in hot weather where the environment temperature may exceed human temperature. In lieu of the aforementioned drawbacks, the design of a low-cost, high-reliability and wide-coverage pedestrian detection system to become a nontrivial task.

In this paper, we aim to design a cost-effective solution for pedestrian detection that can work satisfactorily in almost all roads and weather conditions. Our work forms part of the collective efforts to make our roads smarter whereas smart roads technology would enable AVs to work with IoT sensors and other roadside-integrated technologies to create more efficient and safer driving experience [9]. Considering the problems of pedestrian detection in actual traffic scenario, the objective of the study is to fully exploit the helping role of the "road" as a participant in the traffic network, so that it can actively detect pedestrians and assist AVs via road-vehicle collaboration. To this end, we proposed a highly reliable and cost-efficient IoT-based pedestrian detection scheme using multi-sensor data fusion that allows us to combine the advantages of various sensing technologies while avoiding their shortcomings. Specifically, a low-cost pedestrian detection IoT module integrated with multi-sensor data fusion algorithm is developed to identify pedestrians in road environment, which integrated the high-precision 24GHz Doppler radar, PIR, geomagnetic sensor and so force. By deploying the IoT modules on the road surface, real-time and reliable detection of pedestrians can be achieved, while also provide more timely, accurate and reliable information for vehicles.

The remainder of this paper is organized as follows. Section II introduces hardware design and principle of the system. Section III explains signal processing and multi-sensor data

978-1-7281-5207-3/20/$31.00 ©2020 IEEE

Authorized licensed use limited to: XIDIAN UNIVERSITY. Downloaded on December 25,2020 at 11:01:12 UTC from IEEE Xplore. Restrictions apply.

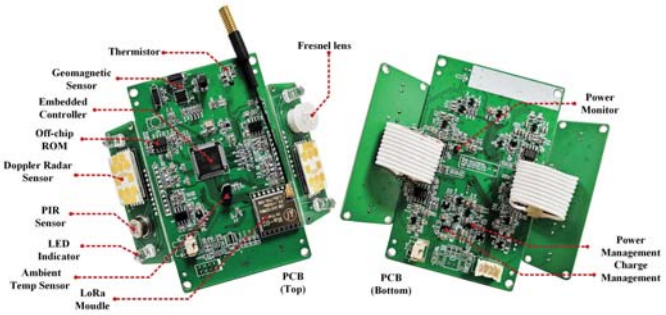

Fig. 1: The iPDM physical board.

fusion based pedestrian detection algorithm in detail. The performance evaluation is described in Section IV, followed by the conclusion in Section V.

II. Hardware Design and Principle

In this section, we introduce the iPDM using multi-sensor data fusion. We will make a brief overview about various sensors' working principle.

A. Hardware of Embedded System

The iPDM is a low-cost, low-power and smart-sensing IoT node powered by a Li-Po and a solar panel, and installed into an enclosure. The nodes are along the two lane lines of a lane in a zig-zag pattern, and the distance between the two nodes on the same lane line is d. Additionally, The iPDM uses low-power LoRa wireless network for communication between peer iPDMs and the base station and organizes into a local area network (LAN) in the form of clusters. The iPDM physical board is illustrated in Fig. 1.

The iPDM is mainly composed of five submodules, including embedded microcontroller, power management submodule, sensors, LED indicator and wireless communication module:

- **Embedded microcontroller:** Its MCU is a 32-bit ARM high-performance microcontroller.
- **Power management:** This submodule consists of Li-Po, solar panel, charge/dischage profile and power monitor. We use MAX17043 Chip as a monitor to prevent deep discharging of Li-Po. As a supplementary source of system energy, a high-efficiency solar panel is adopted to recharge the battery.
- **Sensors:** The core sensor of the module is 24GHz Doppler transceiver. The radiated power (EIRP) of antenna is 12.7dBm, and the corresponding E-plane and H-plane beam widths are about 121° and 111° respectively. The PIR sensor adopted in our module is a general purpose dual elements. It is highly sensitive to human body while remaining insensitive to ambient temperature change, vibration or optical noise. A 3-axis geomagnetic sensor is embedded in iPDM which provides high resolution, low power consumption, large signal noise immunity, a large dynamic range, and high sampling rates. Additionally, a thermistor is used to measure ambient temperature, and a off-chip ROM is employed as backup storage.

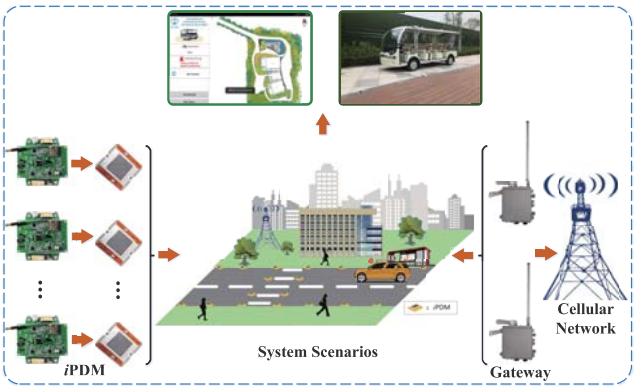

Fig. 2: The architecture diagram of developed system.

- **LED indicator:** Four high-brightness white LEDs are used to alert passing vehicles by flashing lights.
- **Wireless communication:** The wireless communication between iPDMs in the LAN occurs via a LoRa module. Specifically, TDMA is used to intercommunicate in the cluster to avoid message collision. The size of clusters depends on the deployment scenario, and it can support up to 25 nodes, with a typical value of 6.

Additionally, the developed system consists of iPDMs, LoRa gateways, cellular network and cloud server. The AVs rely on LoRa gateways to receive warning signals while human-driven vehicles rely on flashing lights to receive warning signals, and the cloud server completes the reception and management of big data. Note that most local communication is via LoRa gateways or direct communications among iPDMs, and does not have to go through the cloud server. The architecture diagram of developed system is shown in Fig. 2.

B. Detection Principle

1) The Doppler Microwave Radar Sensor: A Doppler microwave radar is a special radar that utilizes the Doppler effect to generate velocity data about targets in some distance away. It does this by transmitting a continuous signal of low-energy microwave radiation and then analyzing the reflected signal. The detector registers a change in the frequency when the radar source and the target are in motion relative to each other. This enables the device to detect moving targets [10]. In the receiver (RX) link, the reflected continuous-wave (CW) signal is then converted into I and Q channels by a quadrature mixer, whereas the reflected local oscillator (LO) signal is converted to a DC offset, which can be easily eliminated by AC coupling. The I/Q mixer output IF$I(t)$ and IF$Q(t)$ can be expressed as

$$\begin{aligned} \mathrm{IF}I(t) &= \mathrm{DC}_I + \mathrm{A}_{IFI} cos[2\pi f_d t + \phi(t)], \\ \mathrm{IF}Q(t) &= \mathrm{DC}_Q + \mathrm{A}_{IFQ} sin[2\pi f_d t + \phi(t)], \end{aligned} \tag{1}$$

where DC_I and DC_Q are the DC offset in I/Q channels, A_{IFI} and A_{IFQ} are the amplitudes of the quadrature output related to the target vibration. $\phi(t) = 4\pi d_0/\lambda + \phi_0$ is the constant phase shift determined by the detection distance d_0 and the phase change ϕ_0 at the reflection surface. f_d is the Doppler frequency derived from the moving target and can be given by

$$f_d \approx 2v\frac{f_t}{c}, \tag{2}$$

Authorized licensed use limited to: XIDIAN UNIVERSITY. Downloaded on December 25,2020 at 11:01:12 UTC from IEEE Xplore. Restrictions apply.

where f_t is the original frequency determined by the radar source, c is the speed of light, and v is the target velocity relative to the source, which is the main parameter to identify the target.

Therefore, based on the quadrature baseband I/Q signals, a mixed reconstructed signal can be obtained by

$$s(t) = \mathrm{IF}I(t) + j \cdot \mathrm{IF}Q(t). \tag{3}$$

In order to obtain Doppler frequency f_d, we need to perform the short-time Fourier transform (STFT) on $s(t)$, shown as

$$S(t,f) = \int s(t') \cdot e^{-(\frac{(t-t')}{2\sigma^2})} \cdot e^{j2\pi f(t-t')} dt' = |\chi| e^{j\theta}, \tag{4}$$

where σ is the time width of a Gaussian window. In the STFT, the frequency-domain resolution is inversely proportional to the time-window size. To extract the unique feature of the Doppler signal of a target in the spectrogram, proper time-window size σ and step size t' should be determined. The pedestrian motion is relatively slow, thus, the STFT will not seriously suffer from a resolution issue in considered scenario.

2) PIR Sensor: A PIR sensor is an electronic sensor that detects infrared (IR) light radiating from targets in its field of view (FoV). They are most often used in PIR-based motion detector, including alarms and automatic lighting applications. PIR sensors detect general movement, but do not give information on who or what moved. A PIR sensor consists of two separate sensing cells, which are placed beneath a rectangular window. The entire sensor is encapsulated in an air-tight metal casing to protect it from environmental interference, such as noise, temperature, humidity and so forth. A moving IR source entering the sensor's FoV will activate the sensing cell one after another, and other IR emitting sources such as ambient IR will affect both cells synchronously and counteract. This creates a difference in temperature between the cells which is converted to an electrical signal by the sensor.

The PIR sensor is fitted with a Fresnel lens to extend its FoV. Fresnel lens can achieve a large aperture and short focal length without significant changes of material. The sensing cells are placed precisely at the focus point of the lens. The FoV of PIR sensor consists of multiple sectors with the detection range varying from one sector to the next, and the image formed by each sector falls on the two sensing cells.

Additionally, the PIR sensor output voltage depends on the characteristics of the target across its FoV, such as the width of the target, distance between the target and the sensor, and velocity of the target. The output voltage of the PIR sensor can be expressed as

$$V_{out} = \beta \cdot a \cdot t \cdot d^{-\alpha} (1 + \frac{|\delta|}{10})^{-\gamma}, \tag{5}$$

where a is the difference in the area of the target's image incident on the two sensing cells, d is the distance of the subject from the PIR sensor, t is the time spent by the target in the FoV of the sensor, δ is the central angle of the FoV sector in which the target is present, and β, α, γ are the adjusting parameters of the sensor [11].

3) Geomagnetic Sensor: Geomagnetic sensors are used to measure the changes of Earth's magnetic field caused by the metal movement, such as passing vehicles, nearby cell phones and computers. The reason for adopting the geomagnetic sensor is that vehicles have a good deal of highly-permeable ferrous materials ($e.g.$, nickel, iron, steel) that cause local disturbance in the Earth's magnetic field flux lines while human body does not cause such local magnetic disturbance. Therefore a geomagnetic sensor allows the separation of vehicles and humans.

Initially, the sensor's calibration state is triggered, and the local magnetic field is sampled without the presence of vehicles. Thus the local reference magnetic flux magnitude $F_{M\mathrm{ref}}(k)$ can be expressed as

$$F_{M\mathrm{r}}(k) = \sqrt{F_{X\mathrm{r}}(k)^2 + F_{Y\mathrm{r}}(k)^2 + F_{Z\mathrm{r}}(k)^2}, \tag{6}$$

where $F_{X\mathrm{r}}(k)$, $F_{Y\mathrm{r}}(k)$, $F_{Z\mathrm{r}}(k)$ are the reference components of the X-axis, Y-axis, Z-axis geomagnetic fields in the kth test, respectively. $F_{M\mathrm{ref}}(k)$ has a Gaussian distribution with a mean of μ and a variance of σ, that is, $F_{M\mathrm{ref}}(k) \propto N(\mu, \sigma)$. Meanwhile, we set a vehicle detection threshold D_{TH} based on the distribution. The initial value is obtained by deploying roadside geomagnetic sensors and collecting geomagnetic data in the field, which can be calculated by

$$D_{TH} = \alpha \times \sigma, \tag{7}$$

where α is an empirical value obtained from a large volume of experimental data. The geomagnetic sensor remains in initial state until condition $F_M(k) \geq D_{TH}$ ($i.e.$, vehicle in detection zone) is met. $F_M(k)$ is calculated as:

$$F_M(k) = \sqrt{(F_X(k) - F_{X\mathrm{r}}(k))^2 + (F_Y(k) - F_{Y\mathrm{r}}(k))^2 + (F_Z(k) - F_{Z\mathrm{r}}(k))^2}, \tag{8}$$

where $F_X(k)$, $F_Y(k)$, $F_Z(k)$ are the instantaneous geomagnetic flux sampling values of X-axis, Y-axis and Z-axis from the sensor [12].

III. Multi-sensor Data Fusion Based Pedestrian Detection Algorithm

In this section, we analyze and process the signal captured from sensors. The embedded system coupled with intelligent algorithms aim to support various complex traffic applications and scenarios.

A. Signal Processing

In this paper, we first collect and process the signal from multiple sensors, and the features of the signal are extracted and analyzed according to Section II. B.

1) Signal Processing of Radar Sensor: To identify a pedestrian using Doppler information, distinguishing features should be extracted from the spectrogram. Firstly, the DC level of I/Q signal are filtered to eliminate their mean value. Then, they were passed through a band-pass filter (BPF) with pass band of 16-1100Hz, based on the frequency of pedestrian moving. At last, the processed I/Q signals are mapped onto time-frequency

Authorized licensed use limited to: XIDIAN UNIVERSITY. Downloaded on December 25,2020 at 11:01:12 UTC from IEEE Xplore. Restrictions apply.

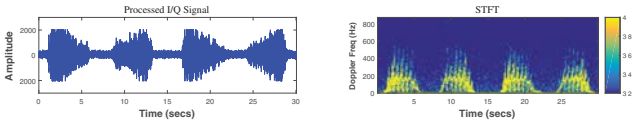

(a) Pedestrian.

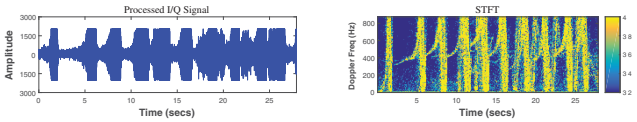

(b) Vehicle.

Fig. 3: Original data and spectrogram of moving targets.

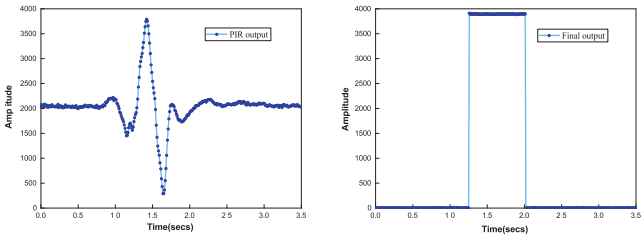

(a) PIR Output. (b) Final Output.

Fig. 4: The output of PIR sensor.

plane using STFT introduced earlier. We extract the maximum instantaneous Doppler frequency. From the intensive tests, we can conclude that a STFT window size of 256 is appropriate to recognize the characteristics in the frequency domain, and a step size of 64 is appropriate for identifying the time-varying Doppler signals with moderate computational complexity. As shown in Fig. 3, the spectrogram of pedestrian and vehicle motion have a distinctive feature with the maximum instantaneous Doppler frequency about 200Hz and 800Hz respectively.

2) Signal Processing of PIR Sensor: In Eq. (5), the empirical values of adjusting parameter β, α and γ are obtained by fitting the equation with the actual output of the sensor from extensive comparative experiments. Here, $\alpha = 1.5$ denotes the rate of output voltage's reduction with distance, $\beta = 11$ is a scale factor, and $\gamma = 10$ determines the amplitude of the peaks of V_{out} [11]. The output of PIR sensor's signal passing through amplifier is shown in Fig. 4(a). In our paper, we also make the PIR output signal pass through a voltage comparator, hence, the final output can be expressed by High/Low levels, as shown in Fig. 4(b), where High-level indicates that a pedestrian has been detected.

3) Signal Processing of Geomagnetic Sensor: The geomagnetic data of X-axis, Y-axis and Z-axis collected by the iPDM are shown in Fig. 5, where Fig. 5(a)-(c) are the geomagnetic signals of a car, minibus and pickup, respectively. The subfigures show that their triaxial geomagnetic signals have distinct features. After that, we calculate the detection threshold $D_{TH} = 90$ based on Eqs. (6)-(7). According to Eq. (8), the triaxial geomagnetic signals of different vehicle types are fused, and the result is shown as Fig. 5(d). At last, we compare $F_M(k)$ with D_{TH} to determine whether there is a vehicle driving away.

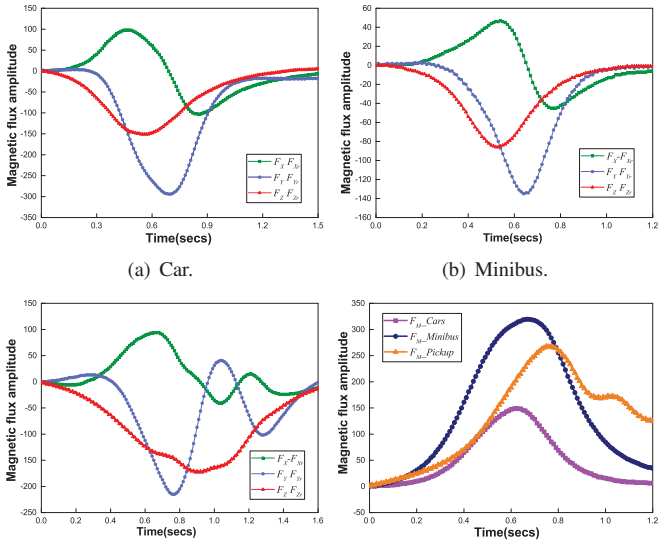

(a) Car. (b) Minibus.

(c) Pickup. (d) Fusion result.

Fig. 5: The output result of geomagnetic sensor.

B. Multi-sensor Data Fusion Algorithm

To realize the real-time pedestrian detection using iPDM nodes, we develop a multi-sensor data fusion algorithm based on the data collected by different sensors. Particularly, we take the ambient temperature value as the control parameter to control the switching between radar sensor and PIR sensor. The reason is that the PIR sensor has pretty low power consumption, but it is prone to error detection when the ambient temperature is high. In addition, geomagnetic sensor assists the detection of radar sensor and PIR sensor by distinguishing the vehicles and pedestrians. The procedure is illustrated in Algorithm 1.

IV. Experimental Evaluation

In this section, we carry out field tests to evaluate the performance of pedestrian detection scheme proposed.

A. Experimental setup

The experimental setup is shown in Fig. 6, We carried out two types of experiments, one is an experiment evaluating the relationship between sensors' detection range and tilt Angle ($i.e.$ the Angle between the sensor plane and the horizontal plane). In this experiment, we first measure the detection distance of the sensor by adjusting the tilt Angle of the Doppler radar and PIR sensor in a single iPDM node. The second experiment focuses on evaluating the detection accuracy of the system under the condition of multi-iPDMs' cooperation when the size of cluster is 6. In particular, we deployed iPDMs along a line, and calculated the detection accuracy of the system by counting the number of times that pedestrians and vehicles triggered LED flashing respectively. We conducted 180 tests in total, divided into six groups.

B. Experimental results

In this subsection, we introduce the experiment results of the proposed pedestrian detection scheme in details. The

Authorized licensed use limited to: XIDIAN UNIVERSITY. Downloaded on December 25,2020 at 11:01:12 UTC from IEEE Xplore. Restrictions apply.

Algorithm 1 The Multi-sensor data fusion Algorithm

Input: Doppler radar signal, PIR signal, Geomagnetic signal, Temperature
Output:Detection result
$iPDM$ $Init.$, $Temp_0 = 40°C$, $Timer_0 = 30min$, $Temp$, $Timer$, D_{TH}, f_d, V_{out}, $F_X(k)$;
while $Timer \leq Timer_0$ **do**
  if $Temp > Temp_0$ **then**
    if $f_d > 0$ && $F_X(k) < D_{TH}$ **then**
      Update detection result.
    end if
  end if
  if $Temp \leq Temp_0$ **then**
    if $V_{out} = 1$ && $F_X(k) < D_{TH}$ **then**
      Update detection result.
    end if
  end if
  Update $Timer$.
end while
$Timer = 0$.
Update $Temp$.

(a) (b)

Fig. 6: Experimental Scenario.

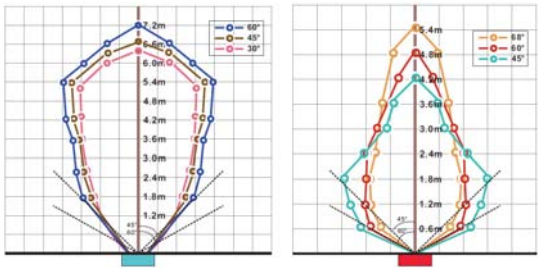

(a) Radar sensor (b) PIR sensor

Fig. 7: The relationship between sensors' detection range and tilt Angle.

relationship between sensors' detection range and tilt Angle is shown in Fig. 7. In this experiment, we conducted three sets of experiments for two main detection sensors to evaluate the impact of tilt Angle on the detection performance of sensors. According to the experimental results, the detection distances of the sensors can reach $7.2m$ and $5.4m$ respectively, and the vertical detection distance will significantly extend with an increase of the tilt Angle. However, the detection Angle of PIR sensor shrinks with an increase of distance. Therefore, in order to ensure that the detection range of the sensor is as large as possible, we unified the tilt Angle of the sensor plane to 45°, and the distance d between two adjacent nodes is set as $8m$.

Additionally, we also show the detection accuracy of the system in Table I. We can see that the detection accuracy of the system tends to be steady, and the final accuracy of the system is 91.7%.

TABLE I: The detection accuracy.

No.	I	II	III	IV	V	VI
Accuracy	0.9	0.87	0.93	0.9	0.97	0.93

V. Conclusion

In this paper, we proposed a IoT-based pedestrian detection scheme using multi-sensor data fusion. In the scheme, we first quantified the output signal by theoretical analysis of the characteristics of the sensor. Then, we developed iPDM hardware system for sensor data capture, processing, feature extraction and fusion. After that, we verified the performance of the system by carrying out field tests. In the end, we concluded that the detection accuracy of the system was 91.7% in the actual traffic scenario.

Acknowledgment

This work was supported by NSFC Projects (U1801266, 61901341), Key R&D Program of Shaanxi (2018ZDXM-GY-038, 2018ZDCXL-GY-04-02), Youth Innovation Team of Shaanxi Universities, and Science and Technology Projects of Xi'an, China (201809170CX11JC12).

References

[1] S. Wang, J. Cheng, H. Liu, F. Wang, and H. Zhou, "Pedestrian detection via body part semantic and contextual information with dnn," *IEEE Transactions on Multimedia*, vol. 20, no. 11, pp. 3148–3159, 2018.
[2] T. Combs, L. Sandt, M. Clamann, and N. McDonald, "Automated vehicles and pedestrian safety: exploring the promise and limits of pedestrian detection," *American journal of preventive medicine*, vol. 56, no. 1, pp. 1–7, 2019.
[3] M. R., "Congress releases guidelines in effort to regulate autonomous vehicles." https://www.govtech.com/fs/Congress-Releases-Guidelines-in-Effort-to-Regulate-Autonomous-Vehicles.html. Published June 15, 2017. Accessed July 13, 2017.
[4] E. Anania, S. Rice, N. Walters, M. Pierce, S. Winter, and M. Milner, "The effects of positive and negative information on consumers willingness to ride in a driverless vehicle," *Transport policy*, vol. 72, pp. 218–224, 2018.
[5] P. Dollar, C. Wojek, B. Schiele, and P. Perona, "Pedestrian detection: An evaluation of the state of the art," *IEEE transactions on pattern analysis and machine intelligence*, vol. 34, no. 4, pp. 743–761, 2011.
[6] X. Liu, K.-A. Toh, and J. Allebach, "Pedestrian detection using pixel difference matrix projection," *IEEE Transactions on Intelligent Transportation Systems*, 2019.
[7] J. Kwon and N. Kwak, "Human detection by neural networks using a low-cost short-range doppler radar sensor," in *IEEE Radar Conference*, 2017, pp. 0755–0760.
[8] B. Mukhopadhyay, S. Sarangi, S. Srirangarajan, and S. Kar, "Indoor localization using analog output of pyroelectric infrared sensors," in *IEEE Wireless Communications and Networking Conference*, 2018, pp. 1–6.
[9] H. Harsono., "Why the worlds first smart highway will most likely be in china." https://techcrunch.com/2019/01/24/why-the-worlds-first-smart-highway-will-most-likely-be-in-china/. Published Jan. 25, 2019.
[10] D. Chang, M. Saito, G. Schultz, and D. Eggett, "Use of hi-resolution data for evaluating accuracy of traffic volume counts collected by microwave sensors," *Journal of Traffic and Transportation Engineering*, vol. 4, no. 5, pp. 423–435, 2017.
[11] B. Mukhopadhyay, S. Srirangarajan, and S. Kar, "Modeling the analog response of passive infrared sensor," *Sensors and Actuators A: Physical*, vol. 279, pp. 65–74, 2018.
[12] W. Balid, H. Tafish, and H. Refai, "Intelligent vehicle counting and classification sensor for real-time traffic surveillance," *IEEE Transactions on Intelligent Transportation Systems*, vol. 19, no. 6, pp. 1784–1794, 2017.

Authorized licensed use limited to: XIDIAN UNIVERSITY. Downloaded on December 25,2020 at 11:01:12 UTC from IEEE Xplore. Restrictions apply.